JGP Journal of General Physiology

RESEARCH ARTICLE

# The rhomboid protease GlpG has weak interaction energies in its active site hydrogen bond network

Kristen A. Gaffney[1] and Heedeok Hong[1,2]

**Intramembrane rhomboid proteases are of particular interest because of their function to hydrolyze a peptide bond of a substrate buried in the membrane. Crystal structures of the bacterial rhomboid protease GlpG have revealed a catalytic dyad (Ser201-His254) and oxyanion hole (His150/Asn154/the backbone amide of Ser201) surrounded by the protein matrix and contacting a narrow water channel. Although multiple crystal structures have been solved, the catalytic mechanism of GlpG is not completely understood. Because it is a serine protease, hydrogen bonding interactions between the active site residues are thought to play a critical role in the catalytic cycle. Here, we dissect the interaction energies among the active site residues His254, Ser201, and Asn154 of *Escherichia coli* GlpG, which form a hydrogen bonding network. We combine double mutant cycle analysis with stability measurements using steric trapping. In mild detergent, the active site residues are weakly coupled with interaction energies ($\Delta\Delta G_{Inter}$) of –1.4 kcal/mol between His254 and Ser201 and –0.2 kcal/mol between Ser201 and Asn154. Further, by analyzing the propagation of single mutations of the active site residues, we find that these residues are important not only for function but also for the folding cooperativity of GlpG. The weak interaction between Ser and His in the catalytic dyad may partly explain the unusually slow proteolysis by GlpG compared with other canonical serine proteases. Our result suggests that the weak hydrogen bonds in the active site are sufficient to carry out the proteolytic function of rhomboid proteases.**

## Introduction

Rhomboid proteases are a unique class of membrane-integrated enzymes that mediate site-specific proteolysis of the membrane-embedded region of integral membrane proteins where water is scarce (Freeman, 2014). Rhomboids are implicated in a variety of regulatory processes by releasing membrane-bound effector proteins including growth factors, transcription factors, or enzymes, which activate them; in *Drosophila melanogaster*, Rhomboid-1 regulates early embryonic development by the cleavage of the membrane-bound epidermal growth factor Spitz (Wasserman et al., 2000; Lee et al., 2001). In yeast, rhomboid Rdb1p regulates mitochondrial remodeling and fusion by the cleavage of GTPase Mgm1p (Sesaki et al., 2003). The mammalian homologue, PARL, serves as an antiapoptotic protein by releasing Opa1 protein into the intermembrane space of the mitochondria to maintain a proper level of cytochrome *c* (Cipolat et al., 2006; Shi and McQuibban, 2017). In *Toxoplasma gondii*, TgROM rhomboids mediate host–cell invasion processes by cleaving adhesins in internal micronemes, which enables their trafficking to the posterior of parasites (Brossier et al., 2005). In the Gram-negative bacterium *Providencia stuartii*, the cleavage of twin-arginine translocase A (TatA), a component of the Tat protein secretion pathway, by AarA rhomboid is required for the production of secreted signaling molecules for quorum sensing (Stevenson et al., 2007).

Mutational and inhibitory studies of Rhomboid-1 first suggested that rhomboids are serine proteases (Urban et al., 2001). Rhomboids possess a unique serine–histidine catalytic dyad (Lemberg and Freeman, 2007) rather than the canonical Ser–His–Asp triad found in other serine proteases (Hedstrom, 2002). Crystallographic studies of the rhomboid protease GlpG from *Escherichia coli* and *Haemophilus influenzae* have revealed that the active site is buried in the protein matrix ∼10 Å below the membrane surface (Wang et al., 2006; Wu et al., 2006; Ben-Shem et al., 2007; Lemieux et al., 2007). These studies also have shown a narrow water-filled cavity contacting the catalytic dyad (Fig. 1). It has been suggested that this cavity serves as a water retention site, which provides water molecules necessary for catalysis (Zhou et al., 2012). Although the molecular details of how rhomboid proteases carry out proteolysis have not been confirmed, a mechanism has been proposed on the basis of in-

[1]Department of Biochemistry and Molecular Biology, Michigan State University, East Lansing, MI; [2]Department of Chemistry, Michigan State University, East Lansing, MI.

Correspondence to Heedeok Hong: honghd@msu.edu.

This work is part of the special collection entitled "Molecular Physiology of the Cell Membrane: An Integrative Perspective from Experiment and Computation."

© 2018 Hong and Gaffney This article is distributed under the terms of an Attribution–Noncommercial–Share Alike–No Mirror Sites license for the first six months after the publication date (see http://www.rupress.org/terms/). After six months it is available under a Creative Commons License (Attribution–Noncommercial–Share Alike 4.0 International license, as described at https://creativecommons.org/licenses/by-nc-sa/4.0/).

Downloaded from http://rupress.org/jgp/article-pdf/151/3/282/1799665/jgp_201812047.pdf by guest on 09 February 2026

hibitory, crystallographic, and enzyme kinetic studies along with comparison to canonical serine proteases (Hedstrom, 2002; Ha, 2007; Vinothkumar et al., 2010, 2013; Xue and Ha, 2012, 2013; Brooks and Lemieux, 2013; Dickey et al., 2013; Zoll et al., 2014; Cho et al., 2016; Tichá et al., 2017). First, the hydrogen bond between catalytic His254 and Ser201 (numbering based on *E. coli* GlpG; $d_{His,N\varepsilon 2\cdots Ser,O\gamma}$ = 2.6 Å) activates the hydroxyl group of the serine for a nucleophilic attack on the carbonyl carbon of the substrate peptide bond to create the first anionic tetrahedral intermediate (Lemberg et al., 2005; Wang et al., 2006). Emerging early as an important residue that may stabilize the intermediate was the conserved asparagine (Asn154) that presumably forms a weak hydrogen bond with the backbone amide group of Ser201 ($d_{Asn,O\delta 1\cdots Ser,N}$ = 3.3 Å). Crystal structures with peptide inhibitors confirmed that the tetrahedral intermediate is stabilized by the interaction with the unique oxyanion triad composed of the conserved Asn154, His 150, and the backbone of the catalytic Ser201 (Xue and Ha, 2012, 2013; Cho et al., 2016). Next, the intermediate is collapsed, resulting in the formal cleavage of the peptide bond and the formation of an acyl enzyme (Vinothkumar et al., 2010, 2013; Xue and Ha, 2012; Brooks and Lemieux, 2013). His254 may then activate a water molecule to initiate the formation of the second tetrahedral intermediate and active site regeneration (Ha, 2007; Xue and Ha, 2012; Brooks and Lemieux, 2013; Vinothkumar et al., 2013). His254 is separated too far from the crystallographic water molecules near the active site (4–5 Å) to mediate the formation of the second tetrahedral intermediate, such that a large conformational change may occur for an optimal rearrangement of the active site (Vinothkumar et al., 2013).

In canonical serine proteases, the catalytic triad (Ser–His–Asp) forms a tight hydrogen bond network, which coordinates a charge relay necessary for catalysis (Hedstrom, 2002). For example, in chymotrypsin, the strong hydrogen bond between His57 and Asp102 is known to facilitate the nucleophilic attack of Ser195 on the substrate peptide bond and stabilizes the doubly protonated form of His57 (Frey et al., 1994). However, it has been argued whether strong hydrogen bonds are necessary between Ser195 and His57 as well as between His57 and Asp102 for catalysis, or whether weak hydrogen bonds are sufficient (Warshel and Papazyan, 1996; Ash et al., 1997; Stratton et al., 2001; Fuhrmann et al., 2006; Ishida, 2006; Tamada et al., 2009; Petrillo et al., 2012; Agback and Agback, 2018). Therefore, measuring the hydrogen bond strengths in the active site network has been a focus of numerous studies (Frey et al., 1994; Markley and Westler, 1996; Ash et al., 1997; Cleland et al., 1998; Lin et al., 1998; Lau and Bruice, 1999; Frey, 2004; Zheng et al., 2006). Rhomboid proteases lack aspartate, which implies that His254 alone should be sufficient to carry out the activation of Ser201 as well as the subsequent charge relay as a general base. Therefore, measuring the strengths of the active site hydrogen bonds is an important task toward understanding the mechanism of proteolysis mediated by rhomboid proteases.

In this study, we determined the pairwise interaction energies between the active site residues (His254, Ser201, and Asn154) of *E. coli* GlpG using double mutant thermodynamic cycles combined with stability measurement directly under mild *n*-dodecyl-β-D-maltopyranoside (DDM) micellar conditions without using chemical denaturants. Interestingly, we show that the catalytic residues in a rhomboid protease are engaged by weak hydrogen bonding interactions compared with those in the canonical serine proteases. The bacterial rhomboid GlpG may represent a unique example among serine proteases in which the strong hydrogen bond network is not required for catalytic proteolysis.

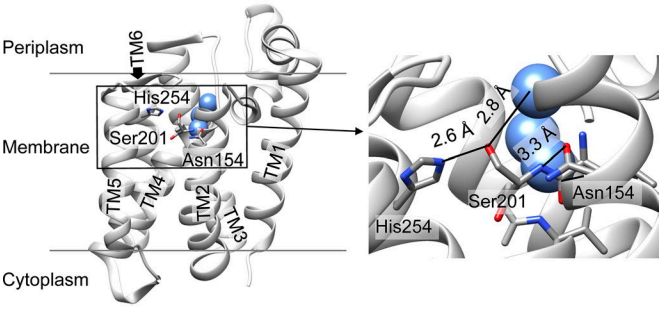


Figure 1. **Hydrogen bond network in the active site of the intramembrane protease GlpG of *E. coli*.** Structure of GlpG (PDB accession no. 3B45) showing the location of the active site and the crystallographic water molecules. Ser201 and His254 form a catalytic dyad. The conserved residue Asn154 forms the oxyanion hole together with the backbone amide group of Ser201 and another conserved residue His150 (data not shown).

## Materials and methods

### Expression and purification of GlpG

The transmembrane (TM) domain of GlpG (residues 87–276) encoded by pET15b vector was expressed in *E. coli* BL21(DE3)-RP strain (Agilent Technologies) with an N-terminal $His_6$-tag (Guo et al., 2016). Cells were grown at 37°C in LB media containing 100 mg/l ampicillin until $OD_{600nm}$ = 0.6 was reached. Then the culture was cooled down on ice for 20 min, and 0.5 mM isopropyl β-thiogalactopyranoside (GoldBio) was added to induce protein expression. The cells were further cultured at 15°C for 16 h. After cell lysis, GlpG was purified from the total membrane fraction obtained by ultracentrifugation (50,000 *g* for 2 h; Type 45 Ti rotor; Beckman Coulter) using $Ni^{2+}$-NTA affinity chromatography (Qiagen) after solubilization with 1% DDM (Anatrace). Site-directed mutagenesis was performed using the QuikChange Site-Directed Mutagenesis kit (Agilent Technologies).

### Biotin labeling of GlpG

GlpG was labeled with the thiol-reactive biotin derivative possessing pyrene fluorophore, N-(5-(2-iodoacetamido)-6-oxo-6-(2-(+)-Biotin hydrazinyl)hexyl)-4-(pyren-1-yl)butanamide (BtnPyr-IA; Btn: biotin, Pyr: pyrene, IA: iodoacetmaide; Fig. 2 a; Guo et al., 2016). Purified double-cysteine cysteine variant (P95C/G172C or G172C/V267C; hereafter, P95C/G172C is denoted as $95/172_N$, in which N indicates that two cysteine residues are introduced in the N-terminal half of GlpG, and G172C/V267C is denoted as $172/267_C$, in which C indicates that two cysteine residues are introduced in the C-terminal half) in 0.2% DDM, 50 mM TrisHCl, and 200 mM NaCl, pH 8.0, buffer were diluted to ∼50 µM and incubated with a 10-fold molar excess Tris(2-carboxyethyl)phosphine–HCl (TCEP; Pierce) for 1 h at room temperature. Then, 40 times molar excess of BtnPyr-IA dissolved in DMSO (∼20 mg/ml) was added to the

Downloaded from http://rupress.org/jgp/article-pdf/151/3/282/1799665/jgp_201812047.pdf by guest on 09 February 2026

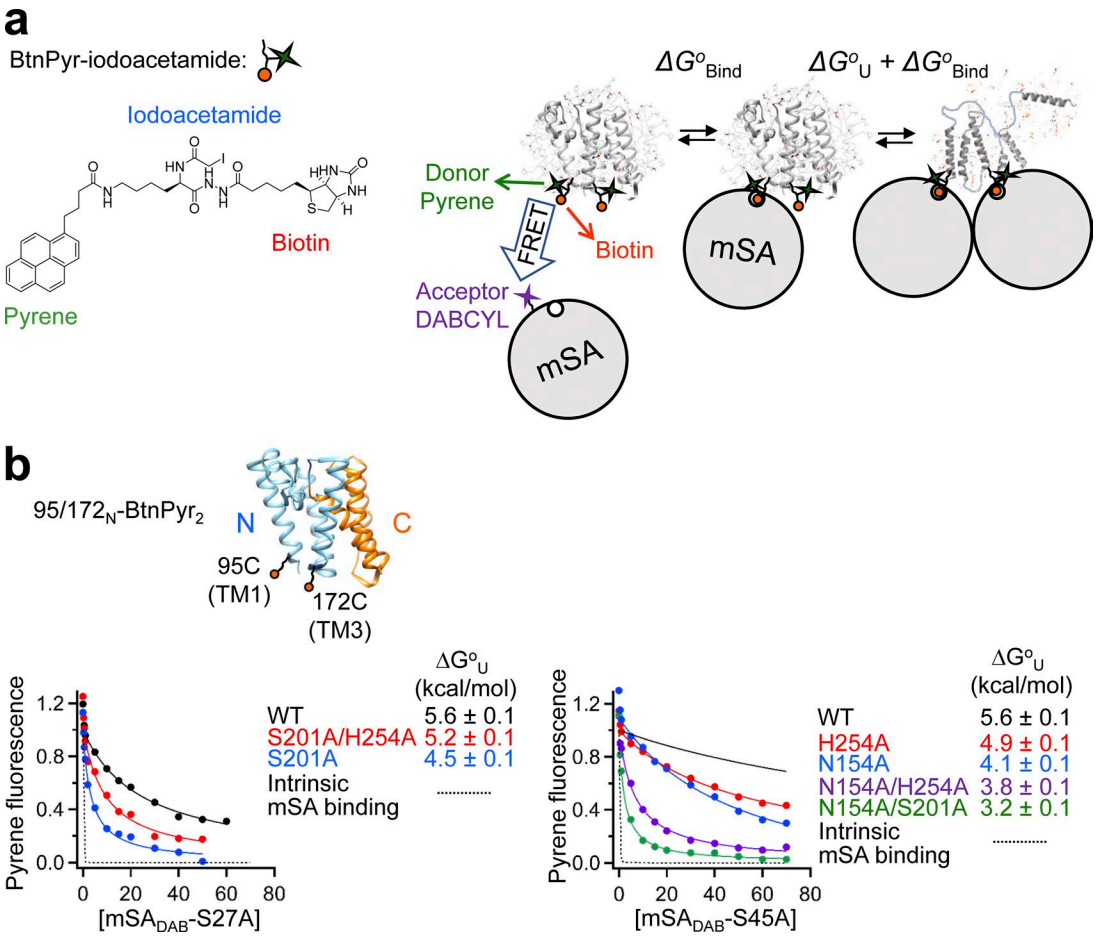


Figure 2. **Measuring thermodynamic stability of GlpG using steric trapping. (a)** Principle of steric trapping. Left: Thiol-reactive biotin derivative with a fluorescent reporter group employed in this study (Guo et al., 2016). Right: When biotin tags are conjugated to two specific residues that are spatially close in the folded state but distant in the amino acid sequence, the first mSA binds either biotin label with the intrinsic binding affinity ($\Delta G^{o}_{Bind}$). Because of steric hindrance, the second mSA binds only when native tertiary contacts are unraveled by transient unfolding. Hence, binding of the second mSA is attenuated depending on the stability of the target protein ($\Delta G^{o}_{Bind} + \Delta G^{o}_{U}$). By adjusting the biotin affinity of mSA by mutation, unfolding and binding reactions can be reversibly controlled, and $\Delta G^{o}_{U}$ of the target protein can be obtained by monitoring binding of the second mSA or protein unfolding. Binding of mSA to biotin labels on GlpG was measured by FRET-based assay using BtnPyr label (donor) and mSA-labeled with nonfluorescent dabcyl quencher (acceptor; Guo et al., 2016). Thiol-reactive dabcyl (DAB-maleimide) was conjugated to a unique cysteine residue (Cys82) engineered in the active subunit of mSA (denoted as $mSA_{DAB}$). **(b)** Binding isotherms between double-biotin variants of GlpG ($95/172_N$-$BtnPyr_2$) and $mSA_{DAB}$ variants with a reduced biotin binding affinity monitored by quenching of pyrene fluorescence. The backbone in cyan: N subdomain (residues 87–198); the backbone in orange: C subdomain (residues 199–276; Guo et al., 2016). Errors in $\Delta G^{o}_{U}$ denote ±SD from fitting. The mSA variant $mSA_{DAB}$-S27A (left, $K_{d,biotin}$ = 1.4 ± 0.9 nM) was used when $\Delta G^{o}_{U}$ of more stable GlpG mutants were measured while $mSA_{DAB}$-S45A (right, $K_{d,biotin}$ = 9.0 ± 4.3 nM) was used for less stable GlpG mutants.

mixture with gentle vortexing. The labeling reaction was incubated in the dark at room temperature overnight. Excess free label was removed by binding the protein to $Ni^{2+}$-NTA affinity resin and washing the bound protein with 0.2% DDM, 50 mM TrisHCl, and 200 mM NaCl, pH 8.0, buffer. Labeled GlpG was passed through a desalting column (EconoPac 10DG; Bio-Rad), which was preequilibrated with 0.2% DDM, 50 mM TrisHCl, and 200 mM NaCl, pH 8.0, buffer to remove imidazole. Typically, the labeling efficiency of BtnPyr-IA ranged from 1.5–2.2 as estimated from the concentration of BtnPyr determined by pyrene absorbance ($\varepsilon_{346nm}$ = 43,000 $M \cdot cm^{-1}$) and the concentration of GlpG determined by Detergent Compatible protein assay (Bio-Rad; Guo et al., 2016).

### Preparation of monovalent streptavidin (mSA)

WT mSA and its variants mSA-S27A and mSA-S45A, in which the mutations were made on the active subunit of tetrameric mSA, were prepared as described previously (Howarth et al., 2006; Hong et al., 2013). Each variant additionally contained a single-cysteine mutation S83C in the active subunit, to which the thiol-reactive dabcyl quencher (DABCYL Plus C2 maleimide; Anaspec) was conjugated for a binding assay between mSA and $GlpG\text{-}BtnPyr_2$ using FRET (Guo et al., 2016).

### Expression and purification of GlpG substrate SN-LYTM2

For the functional assay of GlpG (Fig. S1), we used the second TM domain of the lactose permease of *E. coli* (Akiyama and Maegawa, 2007) fused to staphylococcal nuclease (SN-LYTM2) as a model substrate (Fig. S1 a; Lemmon et al., 1992; Hong et al., 2010). SN-LYTM2 containing the SN domain and C-terminal $His_6$-tag was encoded in pET30a vector (Guo et al., 2016). In the LYTM2 region, a single cysteine was engineered at the five residues upstream from the scissile bond (i.e., P5 position) for labeling with thi-

Downloaded from http://rupress.org/jgp/article-pdf/151/3/282/1799665/jgp_201812047.pdf by guest on 09 February 2026

ol-reactive, environment-sensitive fluorophore iodoacetyl-7-nitrobenz-2-oxa-1,3-diazol (IA-NBD amide; Setareh Biotech). The construct was expressed in BL21(DE3)-RP *E. coli* strain. The protein was expressed, purified, and labeled as described previously (Hong et al., 2013). The cleavage reaction of LYTM2 by GlpG (1 µM) was initiated by addition of 10 times molar excess of NBD-labeled SN-LYTM2 to purified GlpG variants. Time-dependent changes of NBD fluorescence (Fig. S1 b) were monitored in a 96-well plate using a SpectraMax M5e plate reader (Molecular Devices) with excitation and emission wavelengths of 485 nm and 535 nm, respectively. The decrease in fluorescence intensity, which indicates the transfer of the environment-sensitive NBD fluorophore from the hydrophobic micellar phase to the aqueous phase upon cleavage, was normalized to a control sample with NBD-SN-LYTM2 only. The initial slope of fluorescence change versus time represents the substrate cleavage rate.

### Construction of binding isotherm to determine thermodynamic stability of GlpG using steric trapping

Thermodynamic stability ($\Delta G^o_U$) of GlpG in DDM micelles (20 mM) was determined by measuring the attenuated second binding of mSA labeled with dabcyl quencher ($mSA_{DAB}$) to GlpG doubly labeled with BtnPyr ($95/172_N$-$BtnPyr_2$ or $172/267_C$-$BtnPyr_2$) at room temperature (Guo et al., 2016). $mSA_{DAB}$ binding was monitored by quenching of pyrene fluorescence from BtnPyr labels by FRET. 1 µM of $95/172_N$-$BtnPyr_2$ or $172/267_C$-$BtnPyr_2$ was titrated with $mSA_{DAB}$ variant with a reduced biotin binding affinity, $mSA_{DAB}$-S45A ($K_{d,biotin}$ = 9.0 ± 4.3 nM) or $mSA_{DAB}$-S27A ($K_{d,biotin}$ = 1.4 ± 0.9 nM) in 20 mM DDM, 0.25 mM Tris(2-carboxyethyl) phosphine, 20 mM sodium phosphate, and 200 mM NaCl (pH 7.5; Guo et al., 2016). The use of mSA variants was necessary to achieve the reversibility of the second mSA binding to obtain $\Delta G^o_U$. The titrated samples were transferred to a 96-well UV-compatible microplate, sealed with a polyolefin tape, and incubated for 5 d (for $95/172_N$-$BtnPyr_2$) or 2 d (for $172/267_C$-$BtnPyr_2$) at room temperature. Quenching of pyrene-monomer fluorescence at 390 nm was monitored with an excitation wavelength of 345 nm on a SpectraMax M5e plate reader. Data were averaged from three readings. Nonspecific FRET between pyrene and dabcyl was negligible (Guo et al., 2016).

### Fitting of binding isotherm to determine thermodynamic stability of GlpG

The fitting equation to obtain $\Delta G^o_U$ of GlpG using steric trapping was derived based on the following reaction scheme (Blois et al., 2009; Guo et al., 2016):

$$F \cdot mSA \overset{K_U}{\rightleftarrows} U \cdot mSA, \tag{1}$$

where

$$K_U = \frac{[U \cdot mSA]}{[F \cdot mSA]},$$

and

$$U \cdot mSA + mSA \underset{K_{d,biotin}}{\rightleftharpoons} U \cdot 2mSA, \tag{2}$$

where

$$K_{d,biotin} = \frac{[U \cdot mSA][mSA]}{[U \cdot 2mSA]}.$$

F and U denote the folded and unfolded state, respectively. $K_U$ is the equilibrium constant for unfolding of GlpG, and $K_{d,biotin}$ is the dissociation constant for unhindered biotin binding of mSA. The fitting equation for the second mSA binding phase in the binding isotherm was

$$FL = \frac{1}{\left[1 + \left(K_{d,biotin} + \frac{K_{d,biotin}}{K_U}\right)\frac{1}{[mSA]}\right]}(FL_\infty - FL_0) + FL_0, \tag{3}$$

where $FL$ is measured fluorescence intensity, and $FL_0$ and $FL_\infty$ are the fluorescence intensities at [mSA] = 0 and at the saturated binding level, respectively. [mSA] is the total mSA concentration. After obtaining the fitted $K_U$, the thermodynamic stability was calculated using the equation $\Delta G^o_U = -RT \ln K_U$.

### Cooperativity profiling of the active site residues

The following is the method to identify cooperative and localized side-chain interactions that contribute to the protein stability (Guo et al., 2016). To apply this method to GlpG, we first made a single mutation to perturb a specific side-chain interaction in the background of double biotin variants of GlpG, $95/172_N$-$BtnPyr_2$ and $172/267_C$-$BtnPyr_2$. Next, using steric trapping, the stability changes induced by the mutation are measured with two different biotin pairs that are located in the N and C subdomains, respectively. The differential effect of the same mutation on the stability of each subdomain ($\Delta\Delta\Delta G^o_U$) is quantified ($\Delta\Delta\Delta G^o_U$) using Eq. 4:

$$\begin{aligned}&\Delta\Delta\Delta G^o{}_U = \\ &[(\Delta G^o{}_{U,95/172_N\text{-}BtnPyr_2}(WT) - \Delta G^o{}_{U,95/172_N\text{-}BtnPyr_2}(Mut)] \\ &-[\Delta G^o{}_{U,172/267_C\text{-}BtnPyr_2}(WT) - \Delta G^o{}_{U,172/267_C\text{-}BtnPyr_2}(Mut)] = \\ &\Delta\Delta G^o{}_{U,95/172_N\text{-}BtnPyr_2}(WT - Mut) - \Delta\Delta G^o{}_{U,172/267_C\text{-}BtnPyr_2}(WT - Mut).\end{aligned} \tag{4}$$

$\Delta\Delta G^o_{U,95/172N\text{-}BtnPyr2}$(WT-Mut) and $\Delta\Delta G^o_{U,172/267C\text{-}BtnPyr2}$(WT-Mut) designate the stability changes caused by the same mutation in the backgrounds of $95/172_N$-$BtnPyr_2$ and $172/267_C$-$BtnPyr_2$, respectively. If the mutation causes a similar degree of destabilization for both double-biotin variants with a difference smaller than thermal fluctuation energy ($|\Delta\Delta\Delta G^o_U| \le RT$ = 0.6 kcal/mol; $R$: gas constant; $T = 298K$), the mutated site engages in a "cooperative" interaction. Among the cases where $|\Delta\Delta\Delta G^o_U| > RT$, if the mutation preferentially destabilizes the subdomain containing it, the perturbed interactions are "localized" within that subdomain. If the mutation of a residue, which makes its side-chain contacts only with the subdomain containing it, preferentially destabilizes the other subdomain, we define that perturbation as "over-propagated."

### Online supplemental material

Figure S1 displays an activity assay of GlpG WT and active site mutants. Figure S2 displays a comparison of the GlpG structures determined in detergent and bicelles. Table S1 displays stability changes induced by single Ala mutations on the active site residues.

Downloaded from http://rupress.org/jgp/article-pdf/151/3/282/1799665/jgp_201812047.pdf by guest on 09 February 2026

## Results

### Rationale of double mutant cycle analysis

A double mutant cycle involves WT protein, two single mutants, and the corresponding double mutant. If the change in thermodynamic stability ($\Delta G^{\circ}_{U}$) upon the double mutation differs from the sum of the changes caused by the single mutations, the two residues in WT are coupled, and the magnitude of the difference (interaction energy: $\Delta\Delta G_{Inter}$) is related to the strength of interaction between them (Horovitz, 1996), such that

$$\begin{aligned}\Delta\Delta G_{Inter} &= -[(\Delta\Delta G^{\circ}_{U,XY\text{-}XA} + \Delta\Delta G^{\circ}_{U,XY\text{-}AY}) - (\Delta\Delta G^{\circ}_{U,XY\text{-}AY} + \Delta\Delta G^{\circ}_{U,AY\text{-}AA})] \\ &= -[\Delta\Delta G^{\circ}_{U,XY\text{-}XA} - \Delta\Delta G^{\circ}_{U,AY\text{-}AA}] = -[\Delta\Delta G^{\circ}_{U,XY\text{-}AY} - \Delta\Delta G^{\circ}_{U,XA\text{-}AA}], \end{aligned} \quad (5)$$

where X and Y denote a residue pair of interest in WT, and A designates Ala. The thermodynamic scheme using a double mutant is advantageous for quantifying the strength of a specific inter-residue interaction in the context of the native WT structure: a single mutation disrupts not only the interaction between a specific residue pair of interest but also the interaction between the mutated residue and its environment. Also, the single mutation may induce global or local structural relaxation. These energetic contributions other than the specific inter-residue interaction can be subtracted out by measuring the stability change induced by the same mutation in the absence of the partner residue (Eq. 5; Fersht et al., 1992). Double mutant cycle analysis has been widely used to measure the strengths of intramolecular and intermolecular side-chain interactions for both globular and membrane proteins (Serrano et al., 1990, 1991; Doura and Fleming, 2004; Hong et al., 2006, 2007; Harel et al., 2007; Joh et al., 2008; Sokolovski et al., 2017). To minimize the possibility of creating new interactions after mutation, we replaced each active site residue with alanine (Horovitz, 1996).

### Mild destabilization by single alanine mutations in the active site residues

To calculate $\Delta\Delta G_{Inter}$ using double mutant cycle analysis, we measured $\Delta G^{\circ}_{U}$'s of WT, single-Ala, and double-Ala mutants of GlpG using a steric trapping, which couples transient unfolding of a doubly biotinylated protein to double binding of bulky mSA (52 kD; see Fig. 2 a for a more detailed description of the principle; Hong et al., 2010; Guo et al., 2016). Compared with conventional stability measurements using chemical denaturants, this method is advantageous because the protein stability can be directly measured in a native solvent and lipid environment. Previously, we have identified optimal sites of thiol-specific biotinylation on GlpG for steric trapping, P95C/G172C ($95/172_{N}$: N indicates the N-terminal subdomain where a biotin pair is located; Fig. 2 b). The unfolded state trapped with this biotin pair is globally denatured and reversibly refolds to the native state upon addition of excess free biotin to dissociate bound mSA (Guo et al., 2016). For measuring $\Delta G^{\circ}_{U}$ of GlpG, a binding isotherm between doubly biotinylated GlpG and mSA is obtained by using the thiol-reactive biotin derivative with a pyrene fluorophore (BtnPyr) and $mSA_{DAB}$ (Guo et al., 2016; Fig. 2 a). When an $mSA_{DAB}$ variant with a reduced biotin binding affinity is used, the binding isotherm monitored by quenching of pyrene fluorescence displays two-phase mSA binding after the binding equilibrium has been reached: the first mSA tightly binds to either biotin label with an intrinsic binding affinity, and the second mSA binds with a weaker affinity because of the coupling to GlpG unfolding. $\Delta G^{\circ}_{U}$ of GlpG is determined by fitting the second binding phase to Eq. 3 (see "Materials and methods").

The binding isotherms using weaker biotin-binding mSA variants ($mSA_{DAB}$-S27A or $mSA_{DAB}$-S45A; Guo et al., 2016) are shown in Fig. 2 b. The single Ala mutations at the active site residues Ser201, His254, and Asn154 completely abolished GlpG activity, as previously reported (Clemmer et al., 2006; Baker and Urban, 2012; Dickey et al., 2013; Fig. S1 b). In the crystal structures determined in detergent, these residues are completely buried in the protein matrix (Fig. S2 a). $\Delta G^{\circ}_{U}$ of the double-biotin variant without additional Ala mutation (i.e., WT) was 5.6 ± 0.1 kcal/mol. Single mutants S201A and H254A were mildly destabilized with $\Delta\Delta G^{\circ}_{U}$'s of 1.1 ± 0.1 and 0.7 ± 0.1 kcal/mol, respectively. Ala mutation at Asn154 induced larger destabilization with $\Delta\Delta G^{\circ}_{U}$ = 1.5 ± 0.1 kcal/mol. Overall, mutations in the active site did not induce substantial destabilization relative to other previously characterized Ala mutations in the buried region of GlpG, for which $\Delta\Delta G^{\circ}_{U}$ can be as large as ∼4 kcal/mol (Guo et al., 2016). Overall, the mild destabilization by the single active site mutations obtained by steric trapping agrees with previous studies using SDS-induced or irreversible thermal denaturation (Table S1; Baker and Urban, 2012; Paslawski et al., 2015).

Next, the stabilities of double-Ala mutants were measured. Interestingly, the double mutation on the catalytic dyad (S201A/H254A) yielded a smaller decrease in the stability ($\Delta\Delta G^{\circ}_{U}$ = 0.4 ± 0.2 kcal/mol) than individual single mutations ($\Delta\Delta G^{\circ}_{U}$ = 0.7–1.1 kcal/mol), indicating that the double mutation caused a certain extent of structural relaxation. The double mutations N154A/H254A and N154A/S201A induced larger destabilization ($\Delta\Delta G^{\circ}_{U}$ = 1.8–2.4 kcal/mol) than individual single mutations, implying an additive effect of the single mutations.

### Weak interaction energies between the active site residues of GlpG

Next, we determined the interaction strengths ($\Delta\Delta G_{Inter}$) between the active site residue pairs using double mutant cycles (Fig. 3; Horovitz, 1996). From this analysis, Ser201 and His254, which form the catalytic dyad and are engaged in a close hydrogen bond ($d_{His,N\varepsilon 2\cdots Ser,O\gamma}$ = 2.6 Å), favorably interacted ($\Delta\Delta G_{Inter}$ = –1.4 ± 0.2 kcal/mol), whereas the interaction between Ser201 and Asn154, which form a more distant side-chain–backbone hydrogen bond ($d_{AsnO\delta 1\cdots SerN}$ = 3.3 Å), was not significant ($\Delta\Delta G_{Inter}$ = –0.2 ± 0.2 kcal/mol). $\Delta\Delta G_{Inter}$ between His254 and Asn154, which are apparently not engaged in any interaction, was not significant either (–0.4 ± 0.2 kcal/mol).

Hydrogen bonds can be categorized according to the strength of their interaction: weak or conventional (2–12 kcal/mol), strong or low-barrier (12–24 kcal/mol), and very strong or single-well (>24 kcal/mol; Frey et al., 1994). Although favorable, the measured hydrogen bond strength of the His-Ser catalytic dyad of GlpG ($\Delta\Delta G_{Inter}$ ≈ –1.4 kcal/mol) is regarded as weak. This interaction is not only substantially weaker than the His57-Asp102 interaction in the active site of chymotrypsin or α-lytic protease

Downloaded from http://rupress.org/jgp/article-pdf/151/3/282/1799665/jgp_201812047.pdf by guest on 09 February 2026

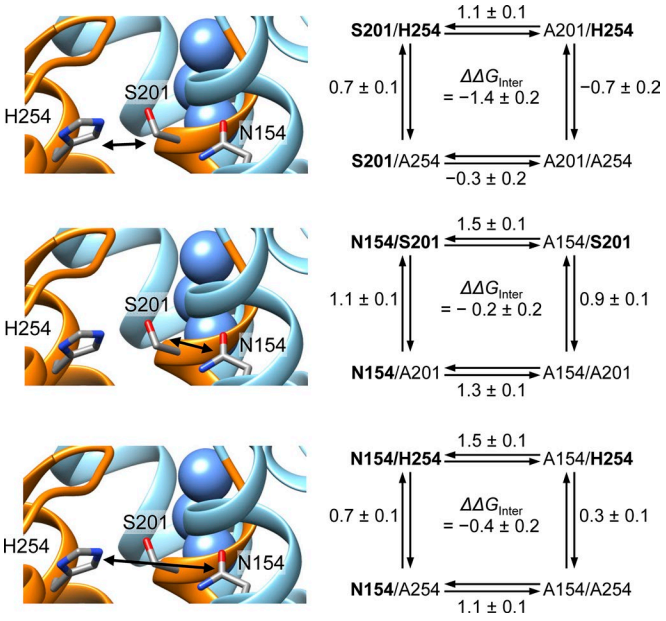


Figure 3. **Double mutant cycle analysis to measure the side-chain interaction energies in the active site of GlpG.** All energy values have units of kcal/mol. The values adjacent to the arrows indicate $\Delta\Delta G^{\circ}_{U}$ induced by the designated mutations. Errors denote ±SD from fitting.

(–5 to –7 kcal/mol before the formation of the first tetrahedral intermediate and –7 to –10 kcal/mol in the first tetrahedral intermediate; Ash et al., 1997; Frey, 2004), which has been suggested to form a low-barrier hydrogen bond, but also weaker than the Ser195-His57 interaction in chymotrypsinogen, classified as moderately strong at an acidic pH (~–13 kcal/mol; Frey et al., 1994; Markley and Westler, 1996).

### Active site residues are involved in cooperative interactions

Finally, we analyzed the contribution of each active site residue to the folding cooperativity of GlpG using the steric trapping-based cooperativity profiling (Fig. 4; Guo et al., 2016). This method is based on the principle that steric trapping captures the transient unfolding of the tertiary interactions in the region to which a specific biotin pair is conjugated. Thus, the local stability of a protein can be measured, and how the local sequence perturbation caused by mutation is propagated throughout the protein structure can be quantified. Briefly, the effect of a specific mutation on the stability ($\Delta\Delta G^{\circ}_{U}$) is measured with two biotin pairs located in different regions. If the difference in the measured stability changes ($\Delta\Delta\Delta G^{\circ}_{U}$) is smaller than thermal fluctuation energy (i.e., $|\Delta\Delta\Delta G^{\circ}_{U}| \leq RT$ = 0.6 kcal/mol), it indicates that the side-chain perturbation by the mutation is propagated evenly throughout the protein and the mutated side chain is engaged in cooperative interactions. If the mutation preferentially destabilizes the subdomain that includes the mutation site ($|\Delta\Delta\Delta G^{\circ}_{U}| > RT$), the mutated side chain is engaged in localized interactions. If the mutation preferentially destabilizes the subdomain that does not include the mutation site with $|\Delta\Delta\Delta G^{\circ}_{U}| > RT$, the mutated side chain is engaged in over-propagated interactions.

To apply this method to the active site residues of GlpG, the stability changes upon each single alanine mutation were measured at the biotin pairs $95/172_{N}$-$BtnPyr_2$ (Fig. 2 b) and $172/267_{C}$-$BtnPyr_2$ (C indicates the C-terminal subdomain in which the biotin pair is located), respectively (Fig. 4 a; Guo et al., 2016). We have shown that the global stability of GlpG is not affected by the presence of these biotin pairs (Guo et al., 2016). S201A mutation at the subdomain interface similarly destabilized the N and C subdomains ($\Delta\Delta G^{\circ}_{U}$ = 1.1 ± 0.1 kcal/mol and 0.6 ± 0.2 kcal/mol, respectively), yielding $|\Delta\Delta\Delta G^{\circ}_{U}| = 0.5 \pm 0.2 < RT$. Thus, Ser201 is classified as cooperatively engaged (Fig. 4 b). Interestingly, H254A mutation in the C subdomain induced destabilization of the N subdomain ($\Delta\Delta G^{\circ}_{U}$ = 0.7 ± 0.1 kcal/mol), whereas the same mutation stabilized the C subdomain containing the mutated site ($\Delta\Delta G^{\circ}_{U}$ = −0.8 ± 0.2 kcal/mol), yielding $|\Delta\Delta\Delta G^{\circ}_{U}|$ = 1.5 ± 0.2 kcal/mol (>2*RT*). Thus, we assign His254 interactions as highly over-propagated. We reason that the stabilization of the C subdomain by the mutation H254A is due to the global structural relaxation induced by the large changes in the side-chain volume and polarity (Fig. 2 b and Fig. 4 b). The mutation N154A preferentially destabilized the N subdomain, where the mutation resides. The resulting $|\Delta\Delta\Delta G^{\circ}_{U}|$of 0.7 ± 0.2 kcal/mol was slightly larger than *RT*. Thus, we assign Asn154 interactions as moderately localized. Our analysis indicates that the absolutely conserved catalytic dyad Ser201–His254 is not only critical for function but also highly communicative with its environment to maintain the folding cooperativity of GlpG.

## Discussion

Here we have shown that the hydrogen bond network in the active site of GlpG is maintained by weak side-chain interactions for its assembly and function. Notably, the strengths of the buried side-chain hydrogen bonds obtained in this study fall into the range of those measured in globular and membrane proteins (0–2.0 kcal/mol; Fleming and Engelman, 2001; Gratkowski et al., 2001; Takano et al., 2003; Hong et al., 2006, 2010; Stanley et al., 2006; Joh et al., 2008; Bowie, 2011; Baker and Urban, 2012). Whereas the previous efforts for membrane proteins have been mainly concerned with "structural" hydrogen bonds that are not directly involved in function, we present the first example of measuring the strengths of "functional" hydrogen bonds conserved in the rhomboid protease family. Our result provides important chemical insights into the initial step of the proteolysis mechanism by rhomboid proteases, i.e., the activation of Ser201 by His254 and the stabilization of the anionic tetrahedral intermediate by Asn154 forming a part of the oxyanion hole. The weak hydrogen bond between His254 and Ser201 must be sufficient to activate Ser201 for the nucleophilic attack on the peptide bond. In addition, the negligible interaction between Asn154 and Ser201 implies that Asn154 will easily gain the flexibility to be adapted to a conformation that can stabilize the oxyanion intermediate.

The kinetic study of GlpG function in the lipid bilayers has shown that the proteolytic activity of GlpG can be characterized as a low substrate-binding affinity ($K_M$ ~135 µM or 0.001 mol fraction, [substrate]/[lipid]), a slow catalytic rate ($k_{cat}$ = 0.0063 $s^{-1}$), and a low efficiency ($k_{cat}/K_M$ ~47 $M^{-1}s^{-1}$) compared with those of other well-studied serine proteases such as chymotrypsin, trypsin, elastase, and α-lytic protease (Dickey et al.,

Downloaded from http://rupress.org/jgp/article-pdf/151/3/282/1799665/jgp_201812047.pdf by guest on 09 February 2026

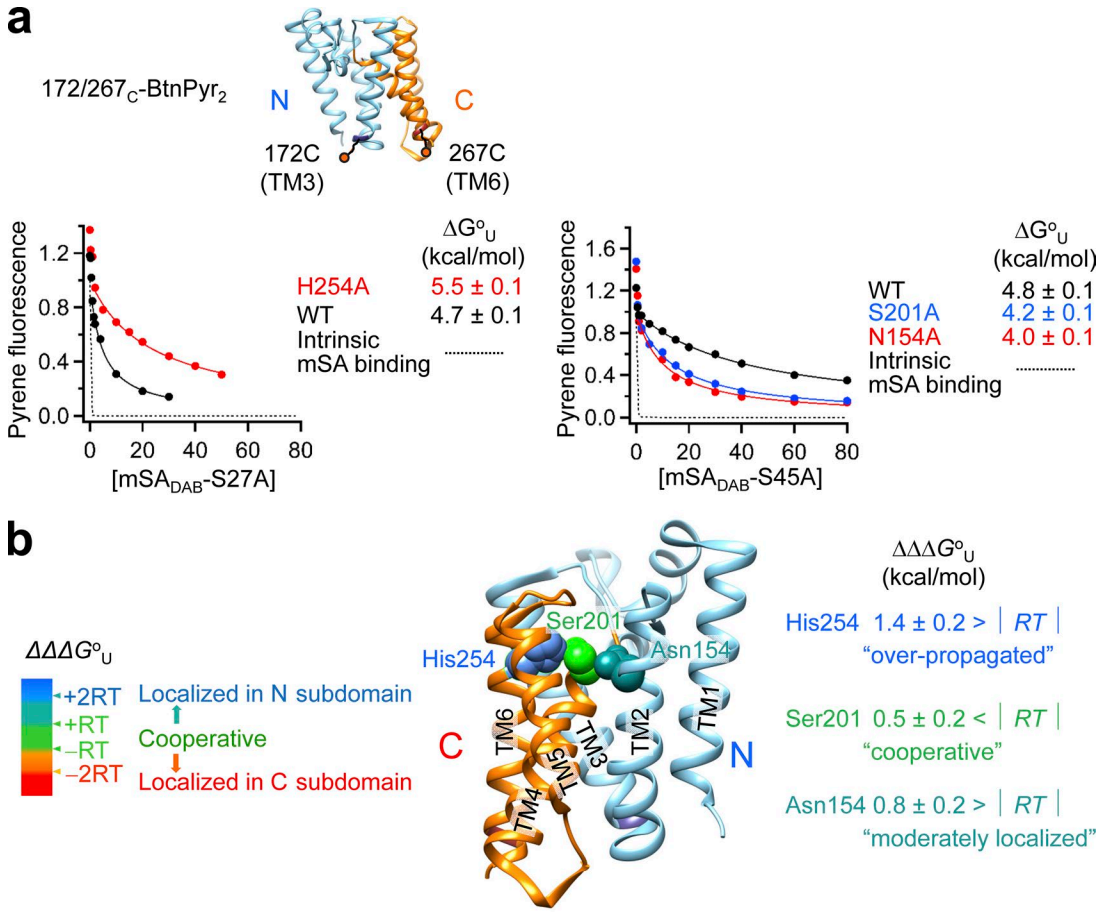


Figure 4. **Cooperativity profiling of the active site residues of GlpG. (a)** Binding isotherms between double-biotin variants of GlpG ($172/267_C$-$BtnPyr_2$) and $mSA_{DAB}$ variants to measure $\Delta G^o_U$ of the C subdomain. **(b)** The cooperativity profiles of the active site residues.

2013). These other proteases, whose catalytic mechanisms are known to be driven by tightly coupled catalytic triads, possess the kinetic parameters of $K_M$ ~$10^1$–$10^4$ μM, $k_{cat}$ ~3–30 $s^{-1}$, and $k_{cat}/K_M$ ~$10^3$–$10^7$ $M^{-1}s^{-1}$ (Brothers and Kostić, 1990; Tsu and Craik, 1996; Coombs et al., 1999). The slow catalytic rate ($k_{cat}$) by GlpG has been mainly attributed to the slow opening of the gating helix TM5, which controls the access of the substrate to the active site in the membrane (Dickey et al., 2013). Although it has been suggested that the hydrolysis reaction is not a rate-determining step responsible for the low $k_{cat}$, the weak hydrogen bond between His254 and Ser201 demonstrated in this study may partly explain the vastly low catalytic ability of GlpG ($10^4$–$10^5$ fold lower $k_{cat}$ than other robust serine proteases).

Here, the side-chain hydrogen bonds were measured in the detergent micellar phase. The possibility remains that the strengths of the same interaction can be different in the lipid bilayers, probably because of the effect of the lateral packing pressure of lipid molecules (Cantor, 1997) as well as the possible difference in the water dynamics that can compete with the active site hydrogen bonds. The thermodynamic stability of helical bundle membrane proteins has been measured in the lipid bilayer environments for the membrane transporter LeuT using urea denaturation (in liposomes), the proton pump bacteriorhodopsin using steric trapping (in DMPC/CHAPSO bicelles), and GlpG using single-molecule force spectroscopy (in DMPC/CHAPSO bicelles; Chang and Bowie, 2014; Min et al., 2015; Sanders et al., 2018). However, the contribution of specific side-chain interactions to the stability has not been quantified in the bilayers. Although the reversible folding of GlpG has not yet been achieved in the bilayer using steric trapping, we expect that the strengths of the hydrogen bonds determined in detergent may not be much different from those in the lipid bilayers for the following reasons. (a) From the crystal structures of GlpG determined in detergent and bilayers (i.e., bicelles), the three active site residues are largely buried in the protein matrix, implying that the inter-residue interactions would be maintained to a similar extent regardless of the surrounding lipid environment (Fig. S2 a; Wang et al., 2006; Vinothkumar, 2011; Cho et al., 2016). (b) The structures of GlpG in detergent and bicelles are virtually identical (Fig. S2, b and c; Wang et al., 2006; Vinothkumar, 2011; Cho et al., 2016). Although the structure of WT in bicelles is not available, the structural comparison of the inactive mutant S201T determined in detergent to that in bicelles indicates that the geometry of the active site residues and the network of the water-mediated hydrogen bonds are similar in the two environments (Fig. S2 b; Vinothkumar, 2011). (c) Although it has been reported that the lipid bilayers enhance the activity of GlpG by ~twofold relative to detergent,

Downloaded from http://rupress.org/jgp/article-pdf/151/3/282/1799665/jgp_201812047.pdf by guest on 09 February 2026

the detergent environment well support the proteolytic activity in a similar timescale (tens of minutes) for known rhomboid substrates (Strisovsky et al., 2009; Baker and Urban, 2012; Moin and Urban, 2012; Xue and Ha, 2013). (d) For the single membrane-spanning TM helices, the strengths of the intermolecular hydrogen bonds determined in detergents are similar to those in the lipid bilayers (1.0 ± 0.5 kcal/mol; Bowie, 2011). For example, the hydrogen bond mediated by glutamate residue in the TM helix of a fibroblast growth factor receptor contributes to the dimer stability by ∼0.7 kcal/mol per monomer in the natural cell membranes (Li et al., 2006). The side chain–backbone intermolecular hydrogen bond mediated by a threonine residue stabilizes the dimer of the glycophorin A TM helix by 1 kcal/mol per monomer (Hong et al., 2010). However, to clarify this issue, it is still necessary to determine the thermodynamic stability of GlpG and the strengths of the hydrogen bonds in a lipid bilayer. Steric trapping is a promising tool to measure the membrane protein stability without disrupting the bilayers. Currently, developing such a protocol for achieving the reversible folding of GlpG in the bilayer is under progress.

## Acknowledgments

We thank Ruiqiong Guo and Miyeon Kim for providing the reagent BtnPyr-IA and critically reading the manuscript.

This work was supported by National Institutes of Health grant R01GM118685, a Michigan State University start-up fund, and the Hunt for a Cure foundation grant RG070103 to H. Hong.

The authors declare no competing financial interests.

Author contributions: K. Gaffney and H. Hong conceived the project and designed experiments. K. Gaffney carried out the experiments and data analysis. K. Gaffney and H. Hong prepared the figures and wrote the manuscript.

José D. Faraldo-Gómez served as editor.

Submitted: 31 August 2018
Accepted: 25 October 2018

## References

Agback, P., and T. Agback. 2018. Direct evidence of a low barrier hydrogen bond in the catalytic triad of a Serine protease. *Sci. Rep.* 8:10078. https://doi.org/10.1038/s41598-018-28441-7

Akiyama, Y., and S. Maegawa. 2007. Sequence features of substrates required for cleavage by GlpG, an Escherichia coli rhomboid protease. *Mol. Microbiol.* 64:1028–1037. https://doi.org/10.1111/j.1365-2958.2007.05715.x

Ash, E.L., J.L. Sudmeier, E.C. De Fabo, and W.W. Bachovchin. 1997. A low-barrier hydrogen bond in the catalytic triad of serine proteases? Theory versus experiment. *Science.* 278:1128–1132. https://doi.org/10.1126/science.278.5340.1128

Baker, R.P., and S. Urban. 2012. Architectural and thermodynamic principles underlying intramembrane protease function. *Nat. Chem. Biol.* 8:759–768. https://doi.org/10.1038/nchembio.1021

Ben-Shem, A., D. Fass, and E. Bibi. 2007. Structural basis for intramembrane proteolysis by rhomboid serine proteases. *Proc. Natl. Acad. Sci. USA.* 104:462–466. https://doi.org/10.1073/pnas.0609773104

Blois, T.M., H. Hong, T.H. Kim, and J.U. Bowie. 2009. Protein unfolding with a steric trap. *J. Am. Chem. Soc.* 131:13914–13915. https://doi.org/10.1021/ja905725n

Bowie, J.U. 2011. Membrane protein folding: how important are hydrogen bonds? *Curr. Opin. Struct. Biol.* 21:42–49. https://doi.org/10.1016/j.sbi.2010.10.003

Brooks, C.L., and M.J. Lemieux. 2013. Untangling structure-function relationships in the rhomboid family of intramembrane proteases. *Biochim. Biophys. Acta.* 1828:2862–2872. https://doi.org/10.1016/j.bbamem.2013.05.003

Brossier, F., T.J. Jewett, L.D. Sibley, and S. Urban. 2005. A spatially localized rhomboid protease cleaves cell surface adhesins essential for invasion by Toxoplasma. *Proc. Natl. Acad. Sci. USA.* 102:4146–4151. https://doi.org/10.1073/pnas.0407918102

Brothers, H.M. II, and N.M. Kostić. 1990. Catalytic activity of the serine proteases alpha-chymotrypsin and alpha-lytic protease tagged at the active site with a (terpyridine)platinum(II) chromophore. *Biochemistry.* 29:7468–7474. https://doi.org/10.1021/bi00484a016

Cantor, R.S. 1997. The lateral pressure profile in membranes: a physical mechanism of general anesthesia. *Biochemistry.* 36:2339–2344. https://doi.org/10.1021/bi9627323

Chang, Y.C., and J.U. Bowie. 2014. Measuring membrane protein stability under native conditions. *Proc. Natl. Acad. Sci. USA.* 111:219–224. https://doi.org/10.1073/pnas.1318576111

Cho, S., S.W. Dickey, and S. Urban. 2016. Crystal Structures and Inhibition Kinetics Reveal a Two-Stage Catalytic Mechanism with Drug Design Implications for Rhomboid Proteolysis. *Mol. Cell.* 61:329–340. https://doi.org/10.1016/j.molcel.2015.12.022

Cipolat, S., T. Rudka, D. Hartmann, V. Costa, L. Serneels, K. Craessaerts, K. Metzger, C. Frezza, W. Annaert, L. D'Adamio, et al. 2006. Mitochondrial rhomboid PARL regulates cytochrome c release during apoptosis via OPA1-dependent cristae remodeling. *Cell.* 126:163–175. https://doi.org/10.1016/j.cell.2006.06.021

Cleland, W.W., P.A. Frey, and J.A. Gerlt. 1998. The low barrier hydrogen bond in enzymatic catalysis. *J. Biol. Chem.* 273:25529–25532. https://doi.org/10.1074/jbc.273.40.25529

Clemmer, K.M., G.M. Sturgill, A. Veenstra, and P.N. Rather. 2006. Functional characterization of Escherichia coli GlpG and additional rhomboid proteins using an aarA mutant of Providencia stuartii. *J. Bacteriol.* 188:3415–3419. https://doi.org/10.1128/JB.188.9.3415-3419.2006

Coombs, G.S., M.S. Rao, A.J. Olson, P.E. Dawson, and E.L. Madison. 1999. Revisiting catalysis by chymotrypsin family serine proteases using peptide substrates and inhibitors with unnatural main chains. *J. Biol. Chem.* 274:24074–24079. https://doi.org/10.1074/jbc.274.34.24074

Dickey, S.W., R.P. Baker, S. Cho, and S. Urban. 2013. Proteolysis inside the membrane is a rate-governed reaction not driven by substrate affinity. *Cell.* 155:1270–1281. https://doi.org/10.1016/j.cell.2013.10.053

Doura, A.K., and K.G. Fleming. 2004. Complex interactions at the helix-helix interface stabilize the glycophorin A transmembrane dimer. *J. Mol. Biol.* 343:1487–1497. https://doi.org/10.1016/j.jmb.2004.09.011

Fersht, A.R., A. Matouschek, and L. Serrano. 1992. The folding of an enzyme. I. Theory of protein engineering analysis of stability and pathway of protein folding. *J. Mol. Biol.* 224:771–782. https://doi.org/10.1016/0022-2836(92)90561-W

Fleming, K.G., and D.M. Engelman. 2001. Specificity in transmembrane helix-helix interactions can define a hierarchy of stability for sequence variants. *Proc. Natl. Acad. Sci. USA.* 98:14340–14344. https://doi.org/10.1073/pnas.251367498

Freeman, M. 2014. The rhomboid-like superfamily: molecular mechanisms and biological roles. *Annu. Rev. Cell Dev. Biol.* 30:235–254. https://doi.org/10.1146/annurev-cellbio-100913-012944

Frey, P.A. 2004. Strong hydrogen bonding in chymotrypsin and other serine proteases. *J. Phys. Org. Chem.* 17:511–520. https://doi.org/10.1002/poc.769

Frey, P.A., S.A. Whitt, and J.B. Tobin. 1994. A low-barrier hydrogen bond in the catalytic triad of serine proteases. *Science.* 264:1927–1930. https://doi.org/10.1126/science.7661899

Fuhrmann, C.N., M.D. Daugherty, and D.A. Agard. 2006. Subangstrom crystallography reveals that short ionic hydrogen bonds, and not a His-Asp low-barrier hydrogen bond, stabilize the transition state in serine protease catalysis. *J. Am. Chem. Soc.* 128:9086–9102. https://doi.org/10.1021/ja057721o

Gratkowski, H., J.D. Lear, and W.F. DeGrado. 2001. Polar side chains drive the association of model transmembrane peptides. *Proc. Natl. Acad. Sci. USA.* 98:880–885. https://doi.org/10.1073/pnas.98.3.880

Guo, R., K. Gaffney, Z. Yang, M. Kim, S. Sungsuwan, X. Huang, W.L. Hubbell, and H. Hong. 2016. Steric trapping reveals a cooperativity network in the intramembrane protease GlpG. *Nat. Chem. Biol.* 12:353–360. https://doi.org/10.1038/nchembio.2048

Downloaded from http://rupress.org/jgp/article-pdf/151/3/282/1799665/jgp_201812047.pdf by guest on 09 February 2026

Ha, Y. 2007. Structural principles of intramembrane proteases. *Curr. Opin. Struct. Biol.* 17:405–411. https://doi.org/10.1016/j.sbi.2007.06.010

Harel, M., M. Cohen, and G. Schreiber. 2007. On the dynamic nature of the transition state for protein-protein association as determined by double-mutant cycle analysis and simulation. *J. Mol. Biol.* 371:180–196. https://doi.org/10.1016/j.jmb.2007.05.032

Hedstrom, L. 2002. Serine protease mechanism and specificity. *Chem. Rev.* 102:4501–4524. https://doi.org/10.1021/cr000033x

Hong, H., G. Szabo, and L.K. Tamm. 2006. Electrostatic couplings in OmpA ion-channel gating suggest a mechanism for pore opening. *Nat. Chem. Biol.* 2:627–635. https://doi.org/10.1038/nchembio827

Hong, H., S. Park, R.H.F. Jiménez, D. Rinehart, and L.K. Tamm. 2007. Role of aromatic side chains in the folding and thermodynamic stability of integral membrane proteins. *J. Am. Chem. Soc.* 129:8320–8327. https://doi.org/10.1021/ja068849o

Hong, H., T.M. Blois, Z. Cao, and J.U. Bowie. 2010. Method to measure strong protein-protein interactions in lipid bilayers using a steric trap. *Proc. Natl. Acad. Sci. USA.* 107:19802–19807. https://doi.org/10.1073/pnas.1010348107

Hong, H., Y.C. Chang, and J.U. Bowie. 2013. Measuring transmembrane helix interaction strengths in lipid bilayers using steric trapping. *Methods Mol. Biol.* 1063:37–56. https://doi.org/10.1007/978-1-62703-583-5_3

Horovitz, A. 1996. Double-mutant cycles: a powerful tool for analyzing protein structure and function. *Fold. Des.* 1:R121–R126. https://doi.org/10.1016/S1359-0278(96)00056-9

Howarth, M., D.J. Chinnapen, K. Gerrow, P.C. Dorrestein, M.R. Grandy, N.L. Kelleher, A. El-Husseini, and A.Y. Ting. 2006. A monovalent streptavidin with a single femtomolar biotin binding site. *Nat. Methods.* 3:267–273. https://doi.org/10.1038/nmeth861

Ishida, T. 2006. Low-barrier hydrogen bond hypothesis in the catalytic triad residue of serine proteases: correlation between structural rearrangement and chemical shifts in the acylation process. *Biochemistry.* 45:5413–5420. https://doi.org/10.1021/bi051515b

Joh, N.H., A. Min, S. Faham, J.P. Whitelegge, D. Yang, V.L. Woods, and J.U. Bowie. 2008. Modest stabilization by most hydrogen-bonded side-chain interactions in membrane proteins. *Nature.* 453:1266–1270. https://doi.org/10.1038/nature06977

Lau, E.Y., and T.C. Bruice. 1999. Consequences of breaking the Asp-His hydrogen bond of the catalytic triad: effects on the structure and dynamics of the serine esterase cutinase. *Biophys. J.* 77:85–98. https://doi.org/10.1016/S0006-3495(99)76874-8

Lee, J.R., S. Urban, C.F. Garvey, and M. Freeman. 2001. Regulated intracellular ligand transport and proteolysis control EGF signal activation in Drosophila. *Cell.* 107:161–171. https://doi.org/10.1016/S0092-8674(01)00526-8

Lemberg, M.K., and M. Freeman. 2007. Functional and evolutionary implications of enhanced genomic analysis of rhomboid intramembrane proteases. *Genome Res.* 17:1634–1646. https://doi.org/10.1101/gr.6425307

Lemberg, M.K., J. Menendez, A. Misik, M. Garcia, C.M. Koth, and M. Freeman. 2005. Mechanism of intramembrane proteolysis investigated with purified rhomboid proteases. *EMBO J.* 24:464–472. https://doi.org/10.1038/sj.emboj.7600537

Lemieux, M.J., S.J. Fischer, M.M. Cherney, K.S. Bateman, and M.N. James. 2007. The crystal structure of the rhomboid peptidase from Haemophilus influenzae provides insight into intramembrane proteolysis. *Proc. Natl. Acad. Sci. USA.* 104:750–754. https://doi.org/10.1073/pnas.0609981104

Lemmon, M.A., J.M. Flanagan, J.F. Hunt, B.D. Adair, B.J. Bormann, C.E. Dempsey, and D.M. Engelman. 1992. Glycophorin A dimerization is driven by specific interactions between transmembrane alpha-helices. *J. Biol. Chem.* 267:7683–7689.

Li, E., M. You, and K. Hristova. 2006. FGFR3 dimer stabilization due to a single amino acid pathogenic mutation. *J. Mol. Biol.* 356:600–612. https://doi.org/10.1016/j.jmb.2005.11.077

Lin, J., C.S. Cassidy, and P.A. Frey. 1998. Correlations of the basicity of His 57 with transition state analogue binding, substrate reactivity, and the strength of the low-barrier hydrogen bond in chymotrypsin. *Biochemistry.* 37:11940–11948. https://doi.org/10.1021/bi980278s

Markley, J.L., and W.M. Westler. 1996. Protonation-state dependence of hydrogen bond strengths and exchange rates in a serine protease catalytic triad: bovine chymotrypsinogen A. *Biochemistry.* 35:11092–11097. https://doi.org/10.1021/bi961366k

Min, D., R.E. Jefferson, J.U. Bowie, and T.Y. Yoon. 2015. Mapping the energy landscape for second-stage folding of a single membrane protein. *Nat. Chem. Biol.* 11:981–987. https://doi.org/10.1038/nchembio.1939

Moin, S.M., and S. Urban. 2012. Membrane immersion allows rhomboid proteases to achieve specificity by reading transmembrane segment dynamics. *eLife.* 1:e00173. https://doi.org/10.7554/eLife.00173

Paslawski, W., O.K. Lillelund, J.V. Kristensen, N.P. Schafer, R.P. Baker, S. Urban, and D.E. Otzen. 2015. Cooperative folding of a polytopic α-helical membrane protein involves a compact N-terminal nucleus and nonnative loops. *Proc. Natl. Acad. Sci. USA.* 112:7978–7983. https://doi.org/10.1073/pnas.1424751112

Petrillo, T., C.A. O'Donohoe, N. Howe, and J.P. Malthouse. 2012. Importance of tetrahedral intermediate formation in the catalytic mechanism of the serine proteases chymotrypsin and subtilisin. *Biochemistry.* 51:6164–6170. https://doi.org/10.1021/bi300688k

Sanders, M.R., H.E. Findlay, and P.J. Booth. 2018. Lipid bilayer composition modulates the unfolding free energy of a knotted α-helical membrane protein. *Proc. Natl. Acad. Sci. USA.* 115:E1799–E1808. https://doi.org/10.1073/pnas.1714668115

Serrano, L., A. Horovitz, B. Avron, M. Bycroft, and A.R. Fersht. 1990. Estimating the contribution of engineered surface electrostatic interactions to protein stability by using double-mutant cycles. *Biochemistry.* 29:9343–9352. https://doi.org/10.1021/bi00492a006

Serrano, L., M. Bycroft, and A.R. Fersht. 1991. Aromatic-aromatic interactions and protein stability. Investigation by double-mutant cycles. *J. Mol. Biol.* 218:465–475. https://doi.org/10.1016/0022-2836(91)90725-L

Sesaki, H., S.M. Southard, A.E. Hobbs, and R.E. Jensen. 2003. Cells lacking Pcp1p/Ugo2p, a rhomboid-like protease required for Mgm1p processing, lose mtDNA and mitochondrial structure in a Dnm1p-dependent manner, but remain competent for mitochondrial fusion. *Biochem. Biophys. Res. Commun.* 308:276–283. https://doi.org/10.1016/S0006-291X(03)01348-2

Shi, G., and G.A. McQuibban. 2017. The Mitochondrial Rhomboid Protease PARL Is Regulated by PDK2 to Integrate Mitochondrial Quality Control and Metabolism. *Cell Reports.* 18:1458–1472. https://doi.org/10.1016/j.celrep.2017.01.029

Sokolovski, M., J. Cveticanin, D. Hayoun, I. Korobko, M. Sharon, and A. Horovitz. 2017. Measuring inter-protein pairwise interaction energies from a single native mass spectrum by double-mutant cycle analysis. *Nat. Commun.* 8:212. https://doi.org/10.1038/s41467-017-00285-1

Stanley, A.M., P. Chuawong, T.L. Hendrickson, and K.G. Fleming. 2006. Energetics of outer membrane phospholipase A (OMPLA) dimerization. *J. Mol. Biol.* 358:120–131. https://doi.org/10.1016/j.jmb.2006.01.033

Stevenson, L.G., K. Strisovsky, K.M. Clemmer, S. Bhatt, M. Freeman, and P.N. Rather. 2007. Rhomboid protease AarA mediates quorum-sensing in Providencia stuartii by activating TatA of the twin-arginine translocase. *Proc. Natl. Acad. Sci. USA.* 104:1003–1008. https://doi.org/10.1073/pnas.0608140104

Stratton, J.R., J.G. Pelton, and J.F. Kirsch. 2001. A novel engineered subtilisin BPN' lacking a low-barrier hydrogen bond in the catalytic triad. *Biochemistry.* 40:10411–10416. https://doi.org/10.1021/bi015542n

Strisovsky, K., H.J. Sharpe, and M. Freeman. 2009. Sequence-specific intramembrane proteolysis: identification of a recognition motif in rhomboid substrates. *Mol. Cell.* 36:1048–1059. https://doi.org/10.1016/j.molcel.2009.11.006

Takano, K., J.M. Scholtz, J.C. Sacchettini, and C.N. Pace. 2003. The contribution of polar group burial to protein stability is strongly context-dependent. *J. Biol. Chem.* 278:31790–31795. https://doi.org/10.1074/jbc.M304177200

Tamada, T., T. Kinoshita, K. Kurihara, M. Adachi, T. Ohhara, K. Imai, R. Kuroki, and T. Tada. 2009. Combined high-resolution neutron and X-ray analysis of inhibited elastase confirms the active-site oxyanion hole but rules against a low-barrier hydrogen bond. *J. Am. Chem. Soc.* 131:11033–11040. https://doi.org/10.1021/ja9028846

Tichá, A., S. Stanchev, K.R. Vinothkumar, D.C. Mikles, P. Pachl, J. Began, J. Škerle, K. Švehlova, M.T.N. Nguyen, S.H.L. Verhelst, et al.2017. General and Modular Strategy for Designing Potent, Selective, and Pharmacologically Compliant Inhibitors of Rhomboid Proteases. Cell Chem. Biol.24:1523–1536e4.

Tsu, C.A., and C.S. Craik. 1996. Substrate recognition by recombinant serine collagenase 1 from Uca pugilator. *J. Biol. Chem.* 271:11563–11570. https://doi.org/10.1074/jbc.271.19.11563

Urban, S., J.R. Lee, and M. Freeman. 2001. Drosophila rhomboid-1 defines a family of putative intramembrane serine proteases. *Cell.* 107:173–182. https://doi.org/10.1016/S0092-8674(01)00525-6

Vinothkumar, K.R. 2011. Structure of rhomboid protease in a lipid environment. *J. Mol. Biol.* 407:232–247. https://doi.org/10.1016/j.jmb.2011.01.029

Vinothkumar, K.R., K. Strisovsky, A. Andreeva, Y. Christova, S. Verhelst, and M. Freeman. 2010. The structural basis for catalysis and substrate spec-

Downloaded from http://rupress.org/jgp/article-pdf/151/3/282/1799665/jgp_201812047.pdf by guest on 09 February 2026

ificity of a rhomboid protease. *EMBO J.* 29:3797–3809. https://doi.org/10.1038/emboj.2010.243

Vinothkumar, K.R., O.A. Pierrat, J.M. Large, and M. Freeman. 2013. Structure of rhomboid protease in complex with β-lactam inhibitors defines the S2′ cavity. *Structure.* 21:1051–1058. https://doi.org/10.1016/j.str.2013.03.013

Wang, Y., Y. Zhang, and Y. Ha. 2006. Crystal structure of a rhomboid family intramembrane protease. *Nature.* 444:179–180. https://doi.org/10.1038/nature05255

Warshel, A., and A. Papazyan. 1996. Energy considerations show that low-barrier hydrogen bonds do not offer a catalytic advantage over ordinary hydrogen bonds. *Proc. Natl. Acad. Sci. USA.* 93:13665–13670. https://doi.org/10.1073/pnas.93.24.13665

Wasserman, J.D., S. Urban, and M. Freeman. 2000. A family of rhomboid-like genes: Drosophila rhomboid-1 and roughoid/rhomboid-3 cooperate to activate EGF receptor signaling. *Genes Dev.* 14:1651–1663.

Wu, Z., N. Yan, L. Feng, A. Oberstein, H. Yan, R.P. Baker, L. Gu, P.D. Jeffrey, S. Urban, and Y. Shi. 2006. Structural analysis of a rhomboid family intramembrane protease reveals a gating mechanism for substrate entry. *Nat. Struct. Mol. Biol.* 13:1084–1091. https://doi.org/10.1038/nsmb1179

Xue, Y., and Y. Ha. 2012. Catalytic mechanism of rhomboid protease GlpG probed by 3,4-dichloroisocoumarin and diisopropyl fluorophosphonate. *J. Biol. Chem.* 287:3099–3107. https://doi.org/10.1074/jbc.M111.310482

Xue, Y., and Y. Ha. 2013. Large lateral movement of transmembrane helix S5 is not required for substrate access to the active site of rhomboid intramembrane protease. *J. Biol. Chem.* 288:16645–16654. https://doi.org/10.1074/jbc.M112.438127

Zheng, Z.L., M.Q. Ye, Z.Y. Zuo, Z.G. Liu, K.C. Tai, and G.L. Zou. 2006. Probing the importance of hydrogen bonds in the active site of the subtilisin nattokinase by site-directed mutagenesis and molecular dynamics simulation. *Biochem. J.* 395:509–515. https://doi.org/10.1042/BJ20050772

Zhou, Y., S.M. Moin, S. Urban, and Y. Zhang. 2012. An internal water-retention site in the rhomboid intramembrane protease GlpG ensures catalytic efficiency. *Structure.* 20:1255–1263. https://doi.org/10.1016/j.str.2012.04.022

Zoll, S., S. Stanchev, J. Began, J. Skerle, M. Lepšík, L. Peclinovská, P. Majer, and K. Strisovsky. 2014. Substrate binding and specificity of rhomboid intramembrane protease revealed by substrate-peptide complex structures. *EMBO J.* 33:2408–2421. https://doi.org/10.15252/embj.201489367

Downloaded from http://rupress.org/jgp/article-pdf/151/3/282/1799665/jgp_201812047.pdf by guest on 09 February 2026